Automated Extraction of Subdural Grid Electrodes from Post-Implant MRI Scans for Epilepsy Surgery

A Thesis
Presented to
The Academic Faculty

by

Maksym O. Pozdin

In Partial Fulfillment
of the Requirements for the Degree
Master of Science in Electrical and Computer Engineering

Georgia Institute of Technology
April 2004

Automated Extraction of Subdural Grid Electrodes from Post-implant MRI scans for Epilepsy Surgery

Approved by:

Dr. Oskar Skrinjar, Advisor

Dr. Anthony Yezzi

Dr. John Oshinski

April 23, 2004

TABLE OF CONTENTS

LIST OF TABLES

LIST OF FIGURES

GLOSSARY

SE: Subdural Electrodes

SGE: Subdural Grid Electrodes

SSE: Subdural Strip Electrodes

CPE: Counter of Positive Edges

SUMMARY

The objective of the current research was to develop an automated algorithm with no or little user assistance for extraction of Subdural Grid Electrodes (SGE) from post-implant MRI scans for epilepsy surgery.

The algorithm utilizes the knowledge about the artifacts created by Subdural Electrodes (SE) in MRI scans. Also the algorithm does not only extract individual electrodes, but it also extracts them as a SGE structures. Information about the number and type of implanted electrodes is recorded during the surgery [1]. This information is used to reduce the search space and produce better results. Currently, the extraction of SGE from post-implant MRI scans is performed manually by a technologist [1, 2, 3]. It is a time-consuming process, requiring on average a few hours, depending on the number of implanted SE. In addition, the process does not conserve the geometry of the structures, since electrodes are identified individually. Usually SGE extraction is complicated by nearby artifacts, making manual extraction a non-trivial task that requires a good visualization of 3D space and orientation of SGE in it. Currently, most of the technologists use 2D slice viewers for extraction of SGE from 3D MRI scans. There is no commercial software to perform the automated extraction task. The only algorithm suggested in the literature is [4]. The goal of the proposed algorithm is to improve the performance of the algorithm in [4].

As a goal, the proposed algorithm performs extraction of SGE not only for individual electrodes, but by applying geometric constraints on SGE.

CHAPTER 1

INTRODUCTION

The objective of the current research was to develop an automated algorithm with no or little user assistance for extraction of Subdural Grid Electrodes (SGE) from post-implant MRI for epilepsy surgery.

The algorithm utilizes the knowledge about the artifacts created by SE in MRI scans. Also the algorithm does not only extract individual electrodes, but it also extracts them as a SGE structures. Information about the number and type of implanted electrodes is recorded during the surgery [1]. This information is used to reduce the search space and produce better results. Currently, the extraction of SGE from post-implant MRI is performed manually by a technologist [1, 2, 3]. It is a time-consuming process, requires on average a few hours, depending on the number of implanted electrodes. In addition, the process does not conserve the geometry of the structures, since electrodes are identified individually. Usually SGE extraction is complicated by nearby artifacts, making manual extraction non-trivial task that requires a good visualization of 3D space and orientation of SGE in it. Currently, most of the technologists use 2D slice viewers for extraction of SSE and SGE from 3D MRI.

There is no commercial software to perform the automated extraction task. The only algorithm suggested in the literature is [4]. The goal of the proposed algorithm is to improve the performance of the algorithm in [4].

As a goal, the proposed algorithm should not only assist technologist working on extraction of SGE, but it should replace him completely and make the process

fully automated. In addition, since the extraction is performed by computer not only individual electrodes are detected, but by applying geometric constraints one can significantly improve the detection of SGE as a structure. Finally, at the final stage technologist can inspect the extracted SGE and make corrections if needed.

Overview of Seizures and Epilepsy Surgery

Epilepsy is a disease that affects approximately 1% of the United States population [5]. It is a process where the patient is having recurrent, unprovoked seizures that originate from a chronic neurological disorder. A seizure is a self-limited event in which a part of the brain is activated uncontrollably. In most of the cases the seizure is triggered by abnormal, disorderly discharging of the brain's nerve cells, resulting in a temporary disturbance of motor, sensory or mental functions [6]. The main causes of seizures are identified as tumor, chemical imbalance, head injuries, certain toxic chemicals or drugs abuse, stroke (hemorrhage), birth injuries [5]. Some seizures involve only a part of the brain and others involve the whole brain. Partial seizures involve a small area of the brain which can then spread to the entire brain, whereas generalized seizures involve the whole brain at once. Treatment options consist of one or more medications and for many people this treatment is sufficient to control their seizures [7]. Unfortunately some patients will continue to have seizures despite taking medications. For such patients an alternative epilepsy treatment is brain surgery. Brain surgery is the only known cure for epilepsy and one of the safest surgeries performed [5].

Even after two or more years of treatment with antiepileptic drugs 20% of the patients still have uncontrollable seizures. Approximately 10% of the epileptic population is good candidate for epilepsy surgery [2]. In 2001 it was estimated that at least 4 million individuals would be seizure free after epilepsy surgery and that less than 0.1% of those potentials candidates have undergone the surgery [5]. These facts indicate that even though epilepsy surgery is beneficial, it still requires improvements in order to gain public awareness and trust.

Epilepsy surgery is a nonreversible procedure that carries certain risk. Successful resection of the brain tissue requires precise localization of the areas of the brain which are the source of the seizures, which are also known as suspected areas. In addition, false or inaccurate localization of the suspected areas can lead to dramatic and undesirable results [8]. Therefore, it is important for successful epilepsy surgery to have the best estimates on the suspected areas.

Once brain surgery is chosen as the method of treatment, the patient undergoes a series of presurgical evaluations and procedures to localize the suspected areas [9]. There is no single procedure that provides sufficient information. Often different procedures that yield similar and repeatable results are used in order to choose the best surgical strategy. Presurgical evaluations typically include several modalities: video-EEG monitoring, MRI, fMRI, SPECT, PET, WADA testing and neuropsychological testing [1, 2, 7, 9]. Additional tests are required to determine if removal of the suspected areas is safe and if it will affect the normal functioning of the brain (motor, sensory, vision and etc) [7].

One of the techniques to localize the suspected areas causing epilepsy is placement of subdural electrodes (SE) on the surface of the brain. SE can be placed with low risk for the patient and can precisely identify seizure areas of the brain [8]. The electrode placement depends on the suspected areas and requires prior evaluations. Most of the time, first approximations about the suspected areas are made from the results of noninvasive evaluations and imaging, MRI, fMRI, PET, SPECT [1, 2, 7, 9].

The approach to place SE varies depending on the size of studied region and number of electrodes to be implanted. In general, SGE are placed through a craniotomy. A part of the skull and bone flaps is removed in order to permit adequate exposure of the brain surface for the electrodes, as well as for the subsequent resection. The dura is then opened and SE are placed over the suspected areas [9]. Most of the time, SGE are placed on either side of the hemisphere and in between two hemispheres as shown on Figure 1.

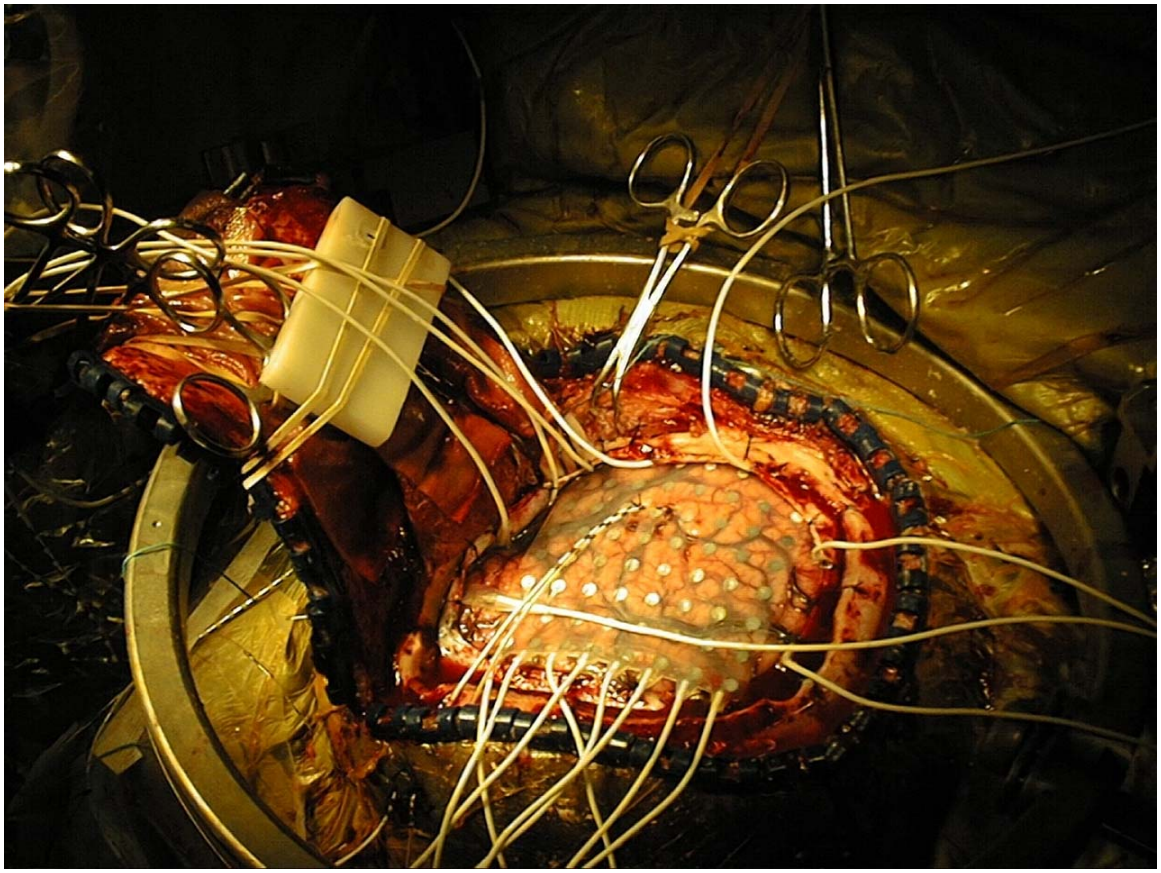

Figure 1. SGE implantation [10]

SSE are placed in difficult to reach areas of the brain surface and can be combined with SGE to cover the suspected areas of the brain. Also, SSE can be implanted not only on the surface but inside the brain. If such need arises, the surgeon performs a small incision and places the SSE inside the tested area [2]. Once adequate coverage has been obtained each electrode wire is individually passed a distance away from the incision to decrease the risk of cerebrospinal fluid leak. Each wire is meticulously secured so it does not become dislodged [6]. The SGE and SSE can be secured directly to the dura to avoid movement during the monitoring period.

The MRI scans are taken before and after the electrode implantation procedure for future monitoring. The post-implant MRI scan is used to extract SE and pin point the location of each electrode on the brain surface. The electrode implantation surgery is safe and patients usually recover within a day or two [5]. For the next two week period they are closely monitored. Electrode recordings on the surface of the brain are correlated with patient's seizures to precisely identify suspected areas of the brain. Based on the EEG recordings during seizure, surgeons are able to conclude which SE are the closest to the affected area and that information is used for brain surgery [9].

Currently the post-implant MRIs are used to perform the mapping from EEG reading of the electrode to the areas on the brain. The process of identifying SE and brain surfaces is performed manually by a technologist. It is a time-consuming and error prone process that requires a good visualization of 3D space and geometric shapes. SE create spherically shaped image artifacts and complicate the process of identifying electrode centers precisely [11].

With these considerations in mind, this research not only helps the technologist to identify SE from post-implant MRI, it also provides accurate information on position and orientation of each SE. Currently there is no commercial software to perform automated extraction of SE. In the literature, there is an algorithm proposed by Dr. Skrinjar [4]. The purpose of this research is to improve the performance of Dr. Skrinjar's algorithm. Another known approach is to extract SE from a post-implant CT [2, 7]. Since CT provides very good contrast between

SE and brain tissue, image artifacts are smaller and extraction process is manually performed by a technologist with better precision. Post-implant CT is not widely used because it exposes the patient to a high level of ionizing radiation and has a poor soft tissue contrast [12].

CHAPTER 2

FUNDAMENTALS ABOUT SUBDURAL ELECTRODES

Terminology

This section deals with the terminology used in association with epilepsy surgery:

Subdural Electrodes (SE) come in two types: Subdural Strips and Subdural Grid Electrodes.

Subdural Strip Electrodes (SSE) – strip of electrodes. The number of electrodes on the strip can vary depending on the size of tested area of the brain [8].

Subdural Grid Electrodes (SGE) – grid of electrodes shown on Figure 2. Typical sizes are 8x8, 8x6, 8x4, 2x10 and vary depending on the investigated area [8].

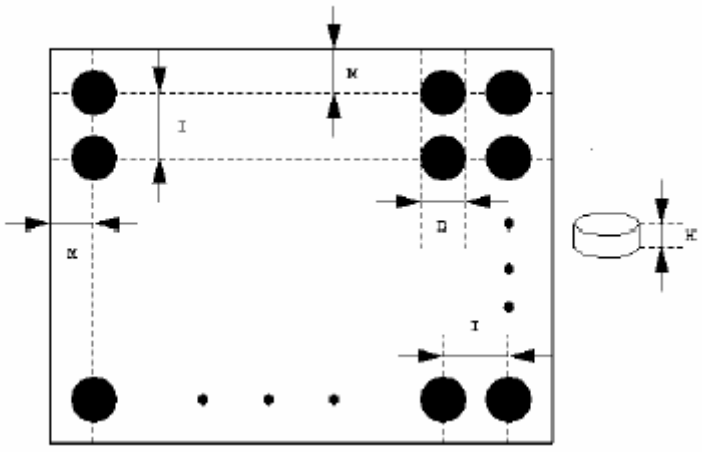

Figure 2. Grid with Subdural Electrodes [4]

Post-implant MRI scans refers to MRI scans taken after SE were implanted [4].

Dark sphere: term used in reference to the sphere-shaped artifact produced by the electrode on the MRI scan. The typical size of the artifact is a sphere with radius

of 3mm and characterized by low intensity. The center of the artifact is superimposed on the center of the electrode.

Subdural Grids and Strips

Before getting into the details of the research, it is essential to discuss the basics of subdural grids and strips. In order to monitor the suspected areas, subdural grids and strips are used. Subdural electrodes are often used because of their ability to cover an extensive brain surface and reliably record seizure activities [5]. In addition, they are easy to implant compared to depth electrodes and they have a low risk of hemorrhage.

A widely used SE type is shown in Figure 3.

Figure 3. An 8x8 SGE

SE can be manufactured by different vendors and under different name, but the basic geometrical shapes and sizes of the electrode disks and the distance between

electrodes is similar. Electrode materials should be a good conductor of electricity, safe for normal brain tissue, MRI and CT safe and resistant to corrosion. The most widely used electrode materials are platinum-iridium alloy and stainless steel. Electrode contacts are usually no more then 2mm in diameter and go from center to center of each electrode. Electrodes and their contacts are embedded in a thin (0.5mm) transparent Silastic plate in which they are laid out in a rectangular array. The Silastic plate serves three specific purposes. First, it is designed to keep electrodes in the fixed distance. Secondly, Silastic plate is flexible enough to be able to wrap any brain surface. Thirdly, it is made transparent to allow a visual inspection of the covered surface area. The electrodes are arranged in a variety of ways to accommodate for different surfaces and sizes [2]. The most common sizes are 8x8, 8x6 and 8x4 (called grids) and 8x1 and 4x1 (called strips). In the instance that the area is not accessible by the grid, such as in between two hemispheres, subdural strips of electrodes are used. It is important to define as much of the suspected areas as possible prior to SE placement. Some of the noninvasive evaluations such as MRI, fMRI, PET, SPECT and skull EEG can be used to localize the suspected areas. For some patients, these techniques have been known to provide little or no information about suspected areas [7]. Often over a hundred SE are placed to cover the suspected areas of seizure origin as determined by noninvasive examination. There are several different approaches to the surgical implantation of SE. A majority of them depend on the investigated area and require a craniotomy [9]. Scalp and bone flaps are cut depending on the investigated area, the dura is

opened and SE are placed by visual inspection. Once the investigated areas are covered with sufficient number of SE arrays, the dura is closed and contacts are carried out to the skull. To prevent movement of SE once the dura and skull are closed, SE can be securely attached to dura [9]. After a successful surgical implantation procedure, the contacts located on the top of the patient's skull are attached to an EEG monitoring unit. The patient is monitored and SE recordings are analyzed for variety of normal and abnormal patterns [7].

The task of precisely identifying the location of SE is difficult. In most cases, post-implant MRI scan of the patient with an SE implant is used to visualize SE and their location. The artifacts of the electrodes in MRI scan make this task difficult [11]. In this research, the electrode artifacts were studied and the algorithm was developed to yield a visualization of SE in post-implant MRI scan. The algorithm was developed to be automatic and requires minimal user interaction to initialize the growing of the grids.

Post-implant MRI scan and Artifacts

In this research T1-weighted MRI scans were used [12]. The algorithm was tested on MRI scans acquired at Emory (Atlanta, GA) and Yale (New Haven, CT) hospitals and should be easily adopted to perform on MRI scans from other hospitals.

An example of post-implant MRI scan is shown on Figure 4.

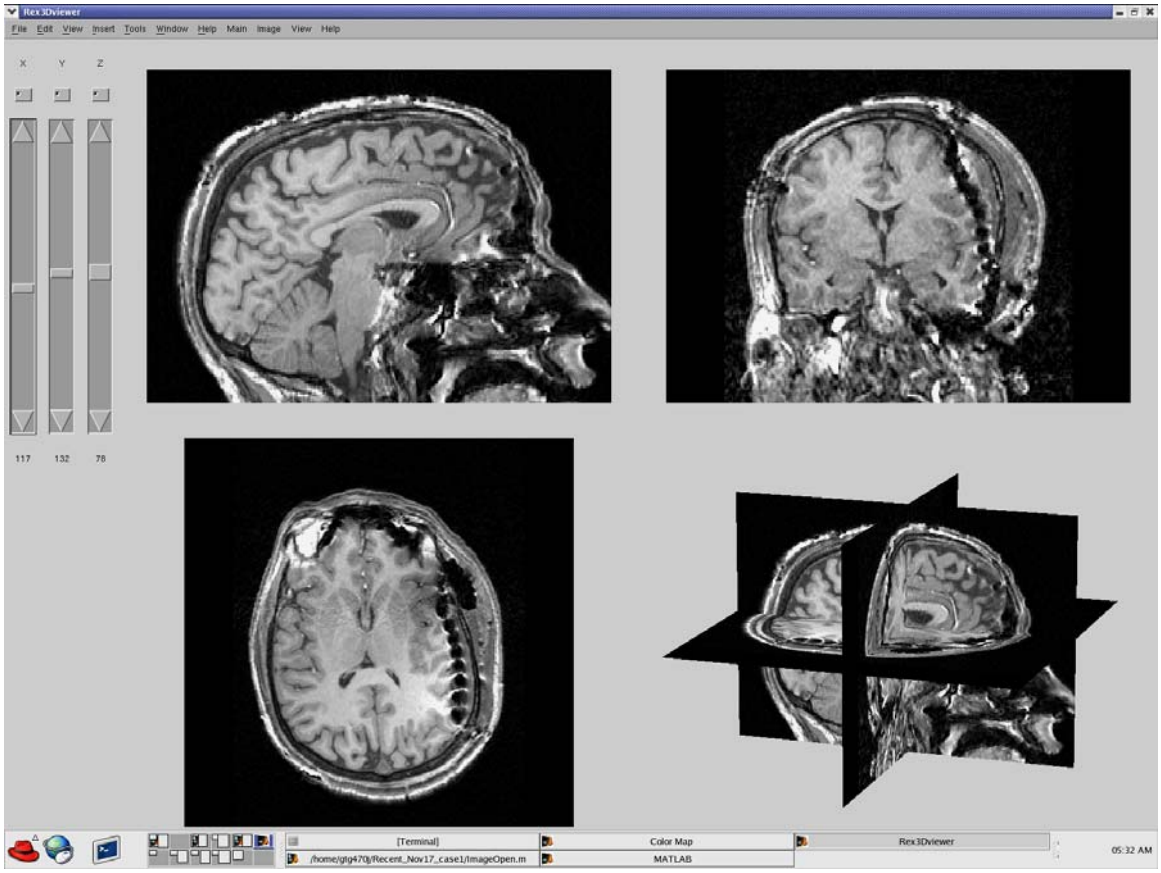

Figure 4. Post-implant MRI scan displayed using Rex3Dviewer

It shows patient's head with internal soft tissue structures. The contrast of MRI scans studied in this research was good. The implanted SE caused image artifacts on the MRI scans. The image artifacts are caused by the corruption of the magnetic field in the MR scanner by the metal electrodes [13]. The nature and cause of the artifacts was not studied in this research. Due to widespread use of existing SE during a surgery, the current research was based on the study of the artifacts and not on their cause.

The artifacts of post-operative MRI scans were studied in-depth and the results are shown in Table 1 and Table 2.

Table 1. Information about SGE and SSE

Geometry of SGE and SSE		
	Disk radius	1.9mm
	Disk width	0.5mm
	Distance between two closest disks	10mm

Table 2. Information about artifacts

Geometry of artifact		
	Shape	Sphere
	Minimum allowed radius of ‘dark spheres’	2.5mm
	Maximum radius of 'dark spheres'	3.5mm
Intensity		
	4mm away from center	below 75%
	7mm away from center	above 75%
SSE structure		
	Minimum distance	6mm
	Maximum distance	14mm
SGE structure		
	Minimum distance	6mm
	Maximum diagonal distance	14mm
	Minimum angle	35 degrees
Thresholds		
	Brain	80%
	Black and White	75%

Structure of Subdural Electrodes

As mentioned earlier there are two types of subdural electrodes: grids and strips. Grids are typically composed of the array of 8x8, 8x6 and 8x4 electrodes. The dimensions and relative sizes for a typical 8x8 grid are shown on Figure 2 and Table 1. Although the electrodes create artifacts in the post-implant MRI scans, dimensions such as the distance between two electrodes and their relative position do not change as shown in Table 2.

Typically strips are used in the areas with limited access or implanted inside the brain for the investigation of suspected areas [5]. The extraction of the strips is easier process than extracting grids. It is primarily due to the fact that the view of the individual electrode artifact in the grid is obstructed by neighboring artifacts. In most cases, the strips that were located in the areas with high contrast did not interfere with other structures and electrode artifacts were easily identified.

Currently, the task of extracting SE from MRI scan is performed by a technologist [11]. This task is time-consuming and error-prone due to noise and distortion caused by artifacts. In addition, it requires a good visualization of 3D space and geometric shapes. In addition, it is non-trivial to estimate the position of the electrodes and their orientation. The goal of this research is to develop a SGE model and then register it on the MRI scan.

CHAPTER 3

DETECTION OF INDIVIDUAL SE

Brief Overview of the Approach

This research was based on the MRI scans provided by Emory (Atlanta, GA) and Yale (New Haven, CT) hospitals. The MRI scans were not identical in terms of the resolution, intensity values, or orientation of the planes. This research was designed to support MRI scans taken with different sequences [11] and it used a few parameters that can be adjusted by the user. Two of these parameters are threshold values for brain segmentation and sphere detection. Currently, the brain threshold is defined as the 80^{th} percentile of the intensity values in MRI scan. This parameter was chosen by tuning. It has a direct relationship to the amount of background present in the MRI scan. The threshold to detect spheres was set to 75^{th} percentile of the intensity values. The brain requires higher threshold values because it appears to be lighter compared to the dark spheres.

All of the programming and algorithm development was performed in MATLAB. MRI data was converted, loaded and displayed using Rex3DViewer program provided by Dr. Skrinjar.

The artifacts created by SE in the MRI scans were studied in depth. Based on that study it was concluded that the artifacts appeared as darker (low intensity) spheres in MRI scans. Therefore, the first step was to find all the dark spheres which could represent SE. The result was presented as a list of 3D coordinates of the centers of the dark spheres. The search for dark spheres yielded the list of

coordinates that contained the centers not only of SE but also of any soft tissue that fit the mask of the dark sphere. It typically contained from of 20,000-50,000 entries with only 100-150 SE present in MRI scan. These results needed additional processing, although there were some important conclusions drawn from it. Most of the SSE were well detected and could be sorted out using a smart search technique. The basic steps of this part of the algorithm are shown on Figure 5.

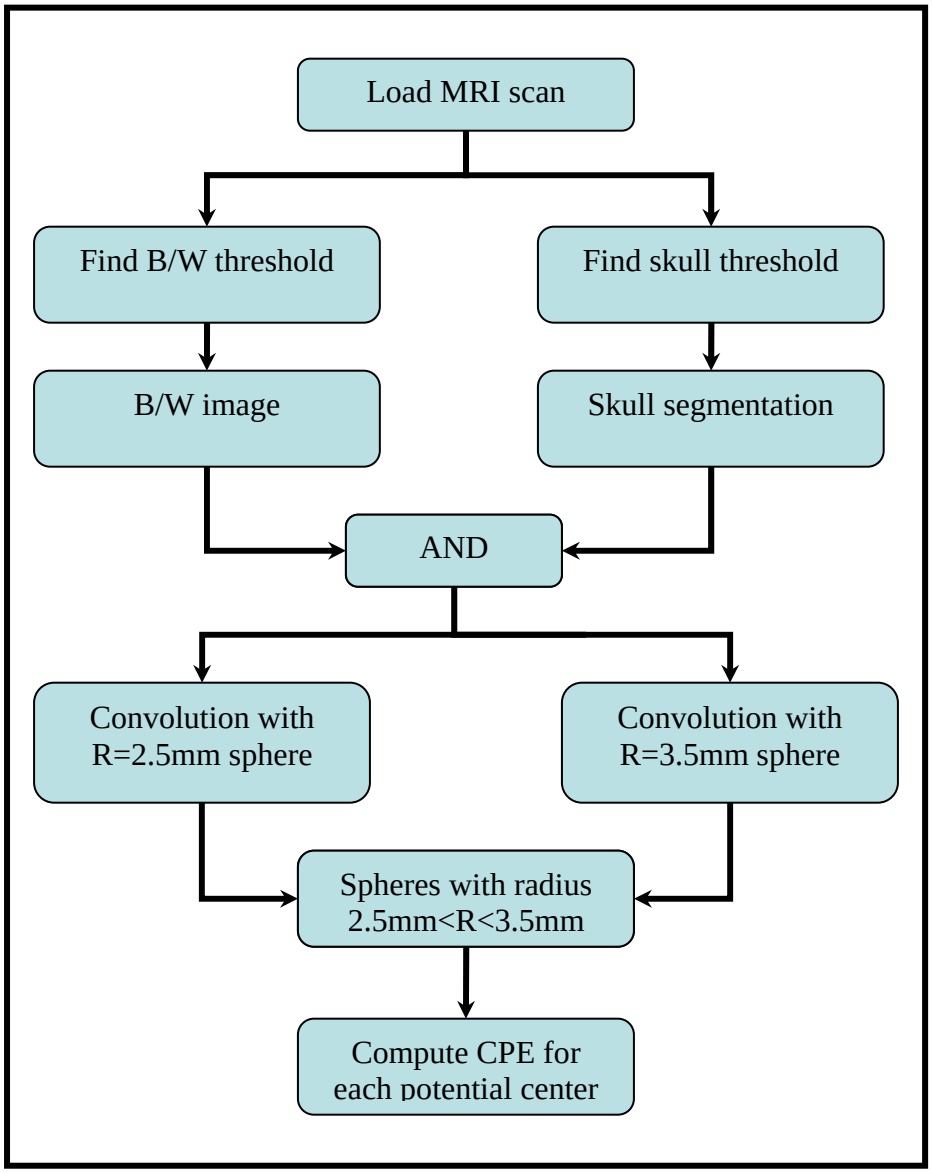

Figure 5. Block diagram of the search algorithm for the dark spheres.

Detection of Dark Spheres

There are various ways to detect dark spheres but in this research the correlation with a mask of the sphere was done [13]. To perform the correlation, a binary convolution of the MRI scan with a sphere mask was performed. Since the sphere

mask is symmetric the results of correlation and convolution are identical. The MRI scan was converted to binary image using dark sphere threshold, where 0 – indicated brighter intensity and 1 – darker intensity.

In addition the skull mask was created to remove outer edges. The skull mask was created by repeated dilation and erosion of the binary scan of the brain. To create the binary scan, the brain threshold was applied since the threshold for dark spheres was too low. Use of a skull mask significantly reduced the amount of false positive detections without removing any information about implanted electrodes. Prior to applying the skull mask some of the false positive results were located on the skull bone, in subdural and subarachnoid spaces. The most successful skull segmentation method was found to be dilation with 3D cross followed by a 3D cube, repeated four times. The largest object was then eroded with 3D cross followed by 3D cube repeated six times [14]. The resulting mask contained the initial MRI scan with an outer skull of approximately 4~6mm removed. Skull mask was combined with a threshold image to perform a search for the dark spheres.

From an extensive analysis of post-implant MRI scans it was concluded that an electrode artifact appears on the scan as a dark sphere (under threshold) and has a radius in the range of 2.5mm and 3.5mm. Therefore the search for the dark spheres with radius of 2.5mm is performed. The result of this search is a list of sphere centers. In order to reduce the number of false positives, a search is performed for the centers of dark spheres with a radius of 3.5 mm. Any center that is common to both lists is removed. This step reduces a list of sphere centers

with 2.5mm radius by at least 30%. This can also lead to losing some of the centers of SE because they were located very close together and could appear as black structures under a threshold and larger than 3.5mm.

A sphere mask is shown in Figure 6.

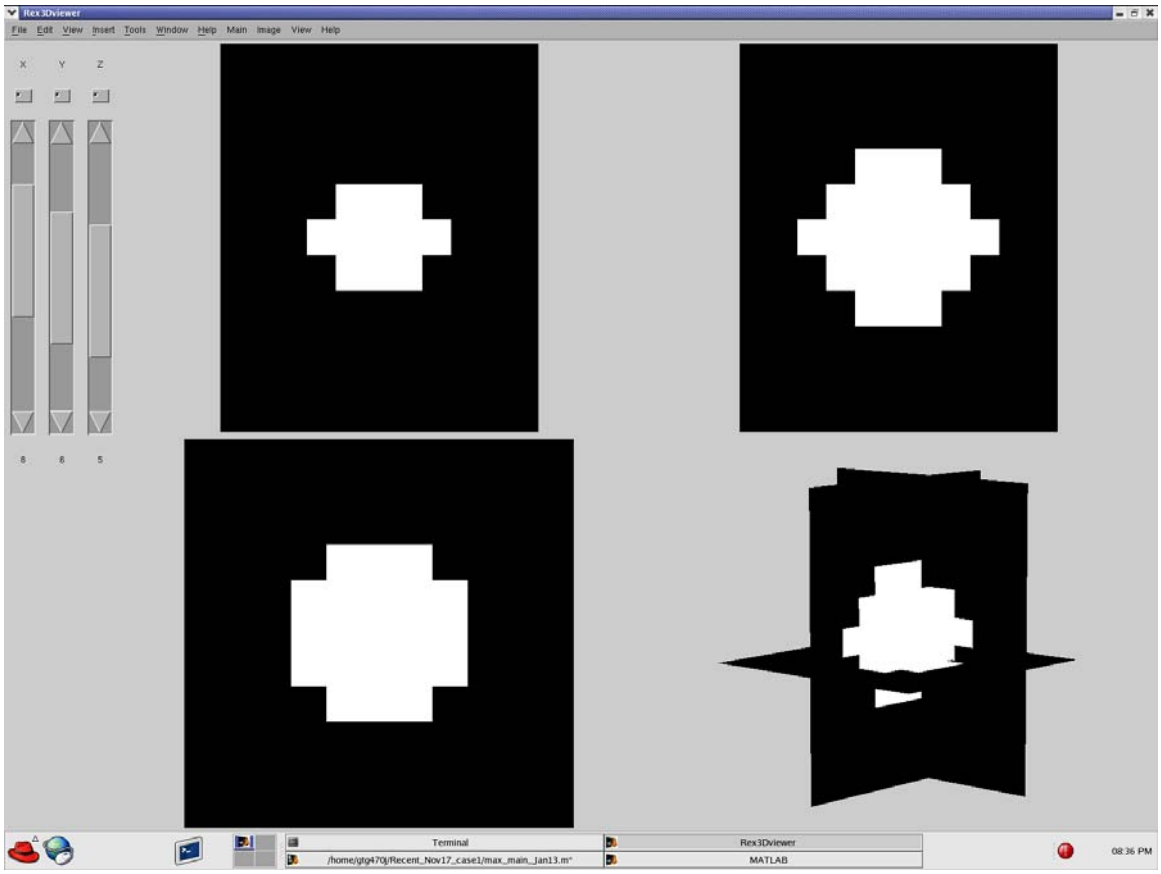

Figure 6. A sphere mask (R=2.5mm)

The mask of the sphere was computed by using sphere equation:

$$x^2 + y^2 + z^2 = R^2$$

The computation was performed for the specified radius, which is one of the parameters. To perform the correlation of the binary scan with the mask, 3D convolution was performed. MATLAB N-dimensional convolution from DSP toolbox was profiled and determined to be slow since it performed convolution in

time domain. To speed up the computation, custom 3D convolution function was written. It performed 3D convolution in the frequency domain, utilizing optimized 3D FFT in MATLAB. The function executed zero pad, 3D FFT, multiplication and 3D IFFT and was significantly faster then N-dimensional convolution function in MATLAB [15]. The computational speed up for a single MRI scan was from 30min to 2min.

The result of convolutions with 2.5mm and 3.5mm was a list of the centers of the potential dark spheres. Although the list was two orders of magnitude bigger then the number of implanted electrodes, it included all the features that were under threshold and had a spherical shape with a radius ranging from 2.5mm to 3.5mm. This list required additional sorting to determine which of these centers could be potential electrodes and which represented noise and other features inside the patient's head. In order to sort the list, the measure value was defined.

Computation of Counter of Positive Edges (CPE)

For each potential electrode center the CPE value was computed. The CPE was designed to correspond to the likelihood that the potential center was the center of the sphere. The idea of CPE was developed based on Hough transform [16]. Based on the artifact geometry from Table 1 the CPE value is defined as the number of intensity changes from bright to dark on the surfaces of two spheres with radii of 7mm and 4mm.

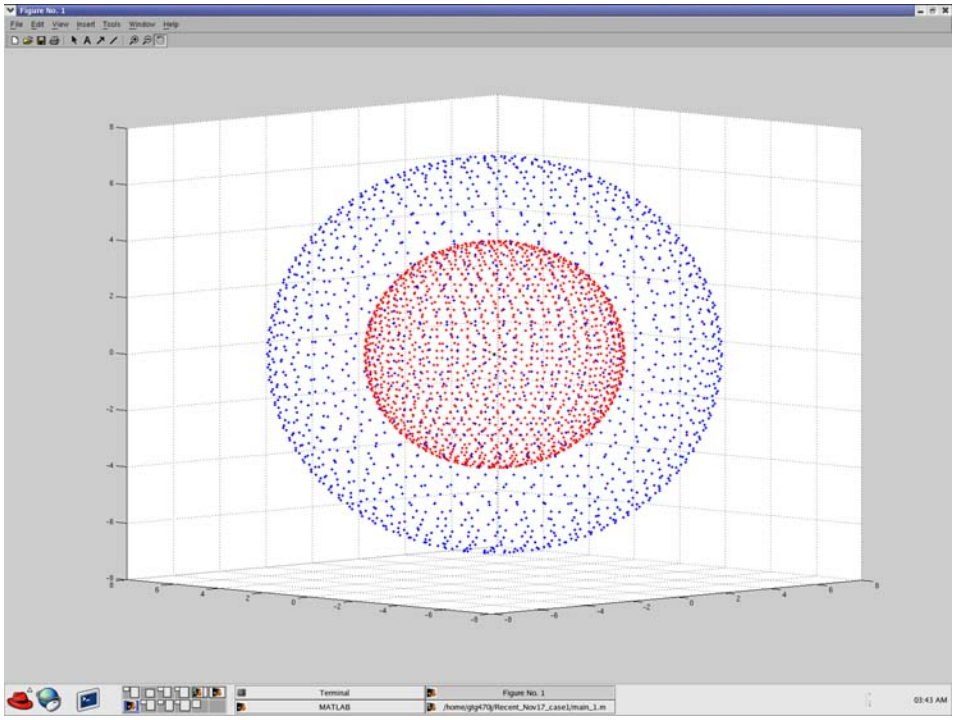

a. Two spheres surfaces (Rin=4 and Rout=7mm)

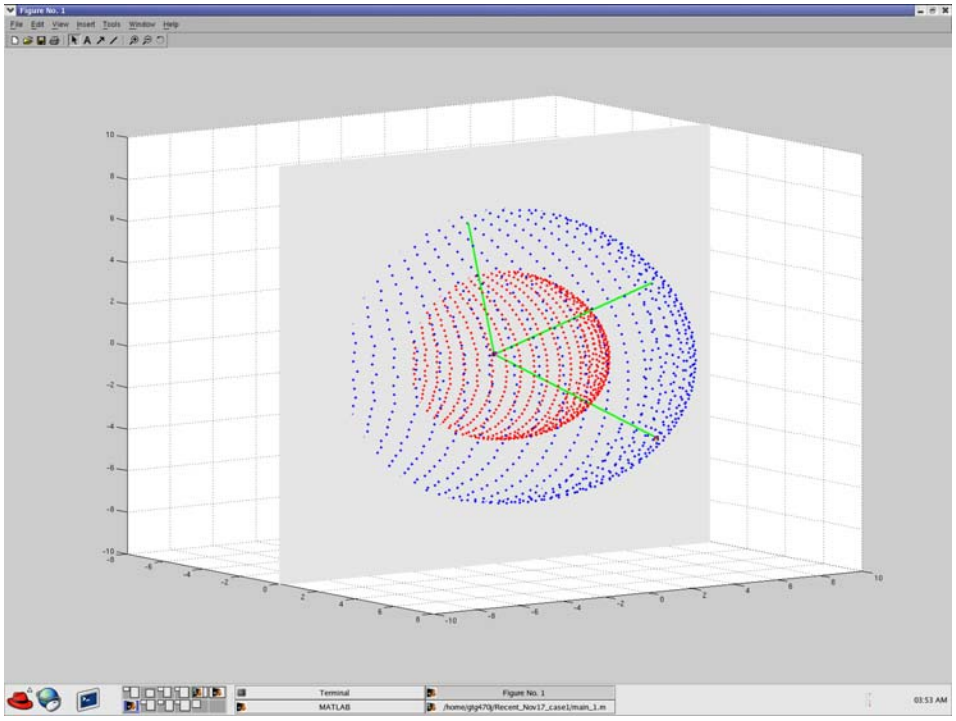

b. Example of CPE computation (intensity change is computed along radial vector shown in green)

Figure 7. Calculation of CPE

There are different ways to define the CPE. Most of them were studied in this research and their performance was compared.

The CPE could represent the change between total intensities on the outer (R=7mm) and inner (R=4mm) spheres. The CPE defined this way was biased towards higher intensity values on outer sphere. In addition, it did not represent individual intensities on the surface of the sphere. The CPE value was cumulatively represented, which could be biased by a high intensity on a side or even on a quarter of the sphere.

The CPE was redefined to represent intensity changes between two spheres along a radial vector that went through the investigated center point and intersected the two spheres. Numerous radial vectors were computed. They were evenly spaced to ensure an even weight in all quadrants of both spheres. The CPE value was computed as a cumulative sum of intensity changes along each vector between the outer and inner sphere. The redefined CPE produced better results than the previous measure, but it still was biased towards high intensity on the outer spheres. Then the CPE was adjusted to count the number of positive edges. Positive edge was defined as positive difference between intensities on the surface of outer and inner spheres along each vector. This CPE put even weight on the positive edges that had relatively high and low difference of intensities. It allowed artifacts that did not have very high intensity changes to have a relatively high measure quantity. This is because the transition from white to black or from gray to black now had even weight [17].

“Smart” Search Technique

A “smart” search technique was successful in SSE detection, but for SGE it was found to be insufficient. The smart search is a sorting technique based on the CPE. The list of the dark sphere centers was sorted based on the CPE values. The first 200 potential centers with the highest CPE were displayed [17]. The only constraint imposed on the displayed points was that they be at least 10mm apart. Since it is known that electrodes placed 10mm apart and that distance is kept fixed (see Table 1). Next, research was concentrated on increasing accuracy and performance in detecting SGE.

CHAPTER 4

DETECTION OF SGE USING A MODEL OF THE GRID

User Interactions

This research aimed to design a fully automated algorithm to extract Subdural Grid Electrodes. However after extensive research and development of different ideas for the algorithm, it was concluded that the extraction of SGE is a non-trivial process and little of user interaction is required to yield best results. The user interaction is required to ensure correct orientation of the model prior to the growing process and this interaction is minimal.

The user is asked to pick a point that is approximately the center of an electrode on the grid. The relative position of the selected electrode to the grid is irrelevant, it is only required for a select electrode to be inside the grid and not on the edges. Once the user has selected an electrode, the algorithm uses it as a center of a 3x3 grid. First, the algorithm attempts to model the 3x3 grid as a plane. Then it uses the plane to initialize the calculations of the grid as a part of the cylinder. Once the calculations have converged, the best fit of 3x3 grid is displayed and the user is asked to confirm that the grid has proper orientation. The confirmation is required due to the fact that a computed grid can possibly have the wrong orientation. The growing process consists of using previous steps and information about initial grids in order to find the whole grid. Therefore, the correct initialization and proper orientation of the initial grid is vital for successful growing. There are two ways for the user to fix the orientation. One way is to

manually adjust the orientation of the grid or ask the user to pick a new point and repeat the computations until a correct orientation is achieved. Since choosing the wrong orientation occurs in one out of five cases, the user is asked to pick a different point on the grid for the purposes of this research. The basic steps for this part of the algorithm are shown on Figure 8.

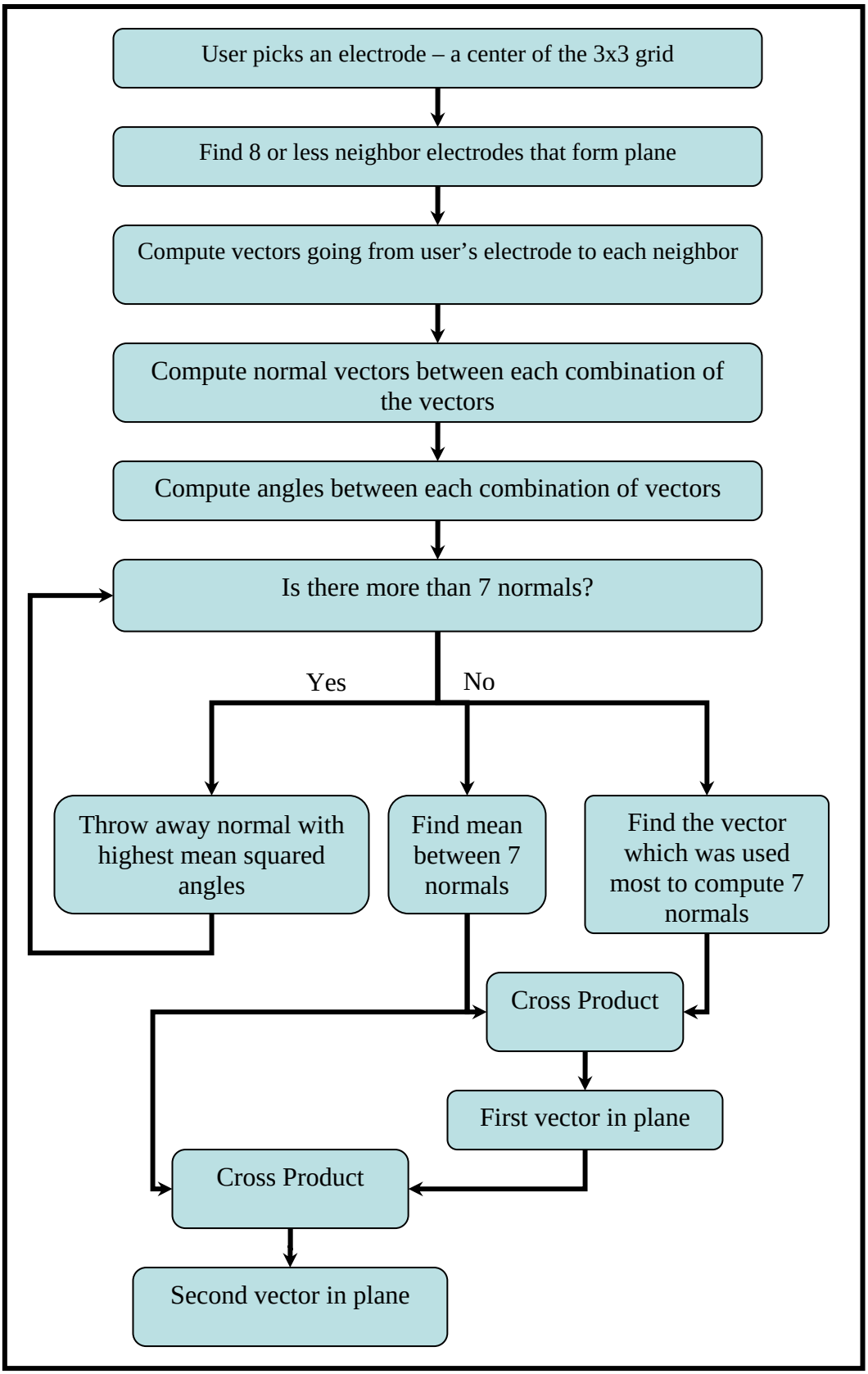

Figure 8. Block diagram to extract 3x3 grid of SE based on the model

Approximating 3x3 grid with a plane

This is the most important step of the extraction of the SGE. Since the results of this step are used for the growing process, it is crucial to perform this step correctly. To ensure that this step is performed accurately, user interaction is required.

First the user is presented with a MRI scan and asked to identify (click or specify) coordinates of a single electrode. This electrode would be used as a center of a 3x3 grid. Therefore the user has to pick an electrode inside the grid and not on the edges. The next steps are based on the assumption that the selected electrode will have 8 neighbors. If the user specifies the electrode on the edge of the grid it could lead to incorrect results and sometimes to complete failure of the algorithm. Although the user specified the position of the electrode, it is only an approximation. Therefore, the user is not required to specify the exact center of the electrode; the algorithm will later adjust the center according to image information.

Once the user has specified the center of the electrode (referred to as the center point) the algorithm will begin searching for the best fit of the 3x3 grid. The first step is to find a best fit for a grid as a flat plane. To specify a plane one needs to know a point and a normal vector [18]. To model grid as a plane, the center point is used as a point on the plane and computation of the normal vector is performed next.

Initially, 8 neighbors are chosen around the center point. The criteria used to select those neighbors are described below.

First, the search space was limited so that it is inside two spheres. The radius of the outer sphere was 14mm and radius of the inner sphere was 6mm. The sizes of the spheres were chosen based on the original grid and maximum/minimum allowed distances between two electrodes (see Table 1 and 2). Second, only potential centers with the highest CPE value were considered. Finally, the potential centers that made an angle between each other and center point of at least 35 degrees were chosen. The result of this step was 8 or less potential centers that were 'dark spheres' and had relatively high CPE. Since some of the potential centers can be missing, the next steps were designed to perform well even for less then 8 neighbors.

Vectors going from the center point to each potential centers were computed. Then a cross product was used to compute the normal between each pair of vectors. For example, if one had 8 potential centers it would yield 28 normal vectors. Although there are 28 normals, only a few of them have approximately the same direction. If a potential center was not located on the plane with others, its normal would be significantly deviated from others. Next, the angles between each normal are computed. Using the computation of mean square deviation from the zero, the vectors with the highest deviation are eliminated until there are only 7 normals left [19]. It is based on the assumption that there are at least 4 potential electrodes that form a plane.

The average between 7 normals is computed, and it is considered to be a normal to the plane. The next step is to compute two orthogonal vectors that span the plane. In this step, 7 normals are analyzed and each vector that was used to

compose those normals is considered. The vector which was used more than any other to compute the normal is considered to be the first vector that spans the plane. The cross product between the normal vector and the first vector is used to compute the second vector. Then the cross product between the second vector and normal is used to refine the first vector. It is performed to ensure that all three vectors are orthogonal [18].

Each vector was normalized. Now there is a center point, and a set of three orthonormal vectors where one is normal to the plane and the other two span the plane. The next step is to find the orientation of the model on the plane. The potential centers used to create the last 7 normals are considered to be a part of 3x3 grid. The model is rotated around the center point and the distance of the model to the closest potential centers is computed. The orientation that yielded the smallest mean square distance is considered the best. The biggest error in this step can happen if the orientation of the 3x3 grid is more then 20 degrees away from the true orientation.

This plane is used to initialize the cylindrical model.

Modeling 3x3 grid as a part of the cylinder

The plane model of 3x3 grid has yielded some important information such as normal and orientation of the model. In addition, it has numerous drawbacks. The plane model does not take into account the curvature or bending of the grid as a whole or just a portion of the grid. Therefore, the next approach was to design a model that would support smooth bending of a grid. The model was developed

based on the knowledge of SGE and their structure. Since SE that formed SGE were embedded in a thin transparent Silastic plate [2] the distances between SE were fixed. In addition, since each SE was connected with a wire, these wires created a flexible canvas for Silastic plate. The canvas was flexible and allowed twisting and bending, but it did not allow stretching/shrinking and flexibility of the canvas was constrained. With the canvas in mind the idea to model a grid as a part of a cylinder was proposed. This model requires more parameters than a plane model. The plane model is used to initialize some of those parameters. In addition to support bending and curving, the model's center point can be adjusted to insure the best registration in the MRI scan. The following parameters are used to implement the cylindrical model [20]:

x_c, y_c, z_c – coordinates of the center point

φ, θ, ψ – orientation of the model (roll, pitch and yaw)

α – orientation of the cylinder, angle between x-axis and central axis of the cylinder

k – curvature, equals to inverse of the cylinder radius

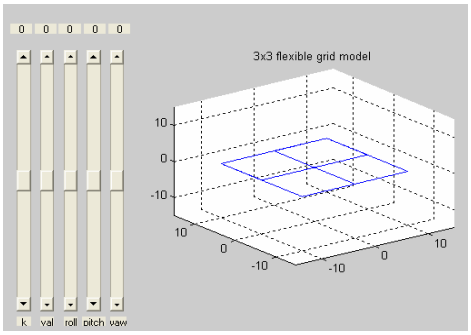

a. k=0, α =0, φ =0, θ =0, ψ =0

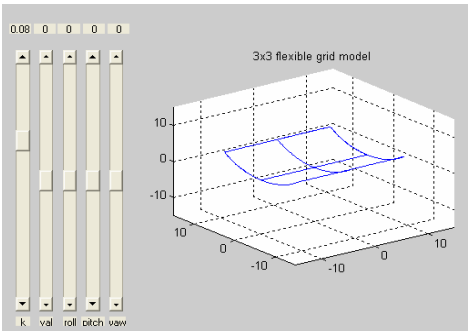

b. k=0.08, α =0, φ =0, θ =0, ψ =0

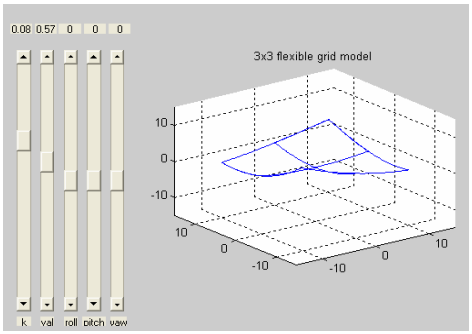

c. k=0.08, α =32^o, φ =0, θ =0, ψ =0

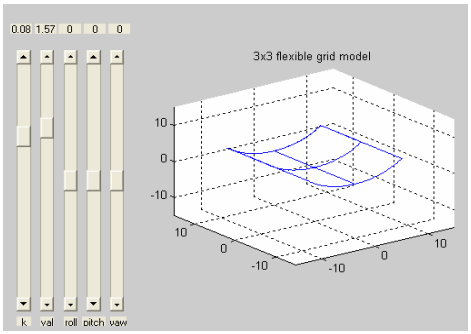

d. k=0.08, α =90^o, φ =0, θ =0, ψ =0

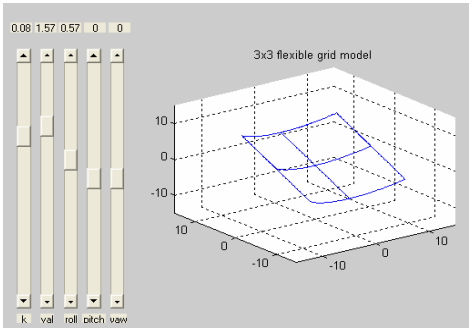

e. k=0.08, α =90^o, φ =32^o, θ =0, ψ =0

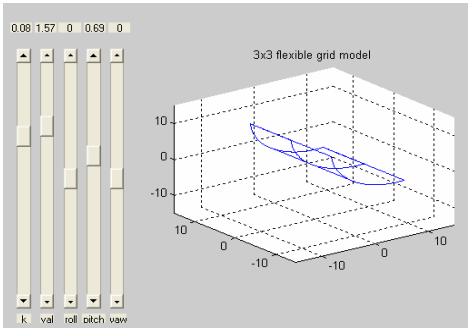

f. k=0.08, α =90^o, φ =0, θ =40^o, ψ =0

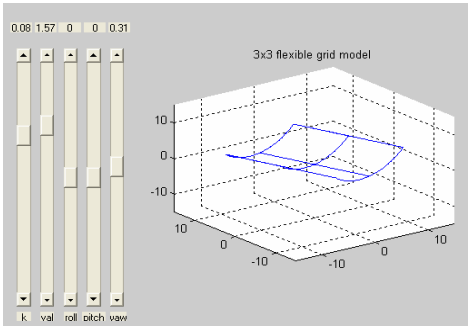

g. k=0.08, α =90^o, φ =0, θ =0, ψ =18^o

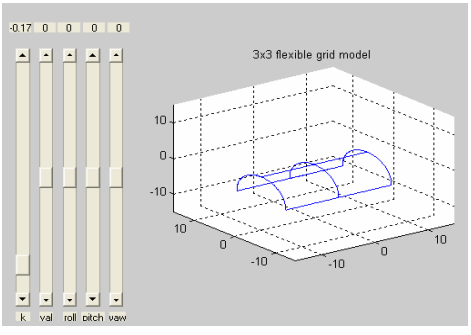

h. k= -0.17, α =0, φ =0, θ =0, ψ =0

Figure 9. Examples of the model with different parameters

The approximation of the grid as a plane has yielded two very important parameters: two orthonormal vectors that span the plane. Those vectors create a local coordinate system (vectors $\vec{u}$ and $\vec{v}$).

The following equations were developed based on the local coordinates and then converted to the global coordinate system of MRI scan [21].

Step 1. Initial rotation of the model prior to applying the curvature:

$$x_1 = u * \cos(\alpha) - v * \sin(\alpha)$$

$$y_1 = u * \sin(\alpha) + v * \cos(\alpha)$$

$$z_1 = 0$$

Step 2. Computation of the model once the curvature was applied:

If k=0

$$x_2 = x_1, y_2 = y_1, z_2 = z_1$$

if $k \neq 0$

$$x_2 = x_1,\ y_2 = \frac{1}{k} * \sin(k * y_1),\ z_2 = \frac{1}{k} * (1 - \cos(k * y_1))$$

Step 3. Undo initial rotation and introduce the angle of cylinder orientation:

$$x_3 = x_2 * \cos(\alpha) + y_2 * \sin(\alpha)$$

$$y_3 = -x_2 * \sin(\alpha) + y_2 * \cos(\alpha)$$

$$z_3 = z_2$$

Step 4. Rotation of the model and translation to global coordinates:

$$\begin{bmatrix} x \\ y \\ z \end{bmatrix} = R(\varphi,\theta,\phi) * \begin{bmatrix} x_3 \\ y_3 \\ z_3 \end{bmatrix} + \begin{bmatrix} x_c \\ y_c \\ z_c \end{bmatrix}$$

where R(φ,θ,ψ) is the rotation matrix. The rotation matrix R can be computed in two ways:

$$R = R(x,\varphi) * R(y,\theta) * R(z,\psi)$$

and this multiplication yields:

$$R(\varphi,\theta,\psi) = \begin{bmatrix} \cos(\psi)*\cos(\theta) & \cos(\psi)*\sin(\theta)*\sin(\varphi) - \sin(\psi)*\cos(\varphi) & \cos(\phi)*\sin(\theta)*\cos(\varphi) + \sin(\phi)*\sin(\varphi) \\ \sin(\psi)*\cos(\theta) & \sin(\psi)*\sin(\theta)*\sin(\varphi) + \cos(\psi)*\cos(\varphi) & \sin(\psi)*\sin(\theta)*\cos(\varphi) - \cos(\psi)*\sin(\varphi) \\ -\sin(\theta) & \cos(\theta)*\sin(\varphi) & \cos(\theta)*\cos(\varphi) \end{bmatrix}$$

where

φ - rotational angle around x-axis

θ - rotational angle around y-axis

ψ - rotational angle around z-axis

in addition R can be specified as

$$R = \begin{bmatrix} u_x & u_y & u_z \\ v_x & v_y & v_z \\ n_x & n_y & n_z \end{bmatrix}, \text{ where}$$

$\vec{u}$, $\vec{v}$ - orthonormal vectors that span a plane

$\vec{n}$ - unit normal vector to the plane.

Gradient ascent search

The 3x3 grid model was created. It was based on the geometric shape and size of SGE. The distance between two neighboring centers was set to 10mm and

diagonal distance was $10 * \sqrt{2}$. The approximation of the grid as a plane was used to compute initial values for roll, pitch and yaw.

To find the best fit of the grid model in MRI scan, the exhausted search for optimum parameters was required. Although after analyzing all eight parameters of the cylindrical model, it was experimentally found that six out of eight parameters, namely roll, pitch, yaw and center point (x_c, y_c, z_c), can be successfully determined by using a gradient ascent search [17]. The cumulative CPE value of all 9 electrodes is used as an energy function for the gradient search. The other two parameters: orientation of the cylinder angle and curvature were determined not to be suitable for the gradient ascent search. It was observed that varying these two parameters by a small amount would not necessarily improve the cumulative CPE.

To perform a search for the best fit of the model in MRI scan orientation of the cylinder angle and curvature were varied independently for a wide range of possible values. The angle of cylinder's orientation was varied from 0^o to 180^o with a step of 18^o. The curvature was varied in the range between -0.09 and 0.09 with the step of 0.01. For a given pair of the cylinder's orientation angle and curvature the gradient ascent search was performed on roll, pitch, yaw and center point. The roll, pitch and yaw were initialized based on the plane model. The CPE value was computed for initial orientation of the model, then one of the angles was varied by $\pm \varepsilon$ keeping other two at their initial value and the CPE values were recorded. Value of ε was set to be arctan(reference_distance/10), where reference_distance is the maximum distance between two closest voxel

centers. The angle increment guarantees that a point 10 mm from center point would move by at least one voxel. Similarly, the CPE computations were repeated for the other two angles, while varying one of them at a time. The CPE values were compared and the direction of the steepest ascent was determined. The values of roll, pitch and yaw were recomputed according the direction of maximum CPE. The roll, pitch and yaw were set to new values and these values would be used for the next iteration. Similar procedure was done for the center point. Initially, the adjustment of the center point (x_c, y_c, z_c) was set to all zeros. Then each coordinate was independently varied by $\pm\Delta$. Value of Δ was set to be reference_distance/6. The value was determined experimentally and chosen to move an investigate point by one voxel. The direction of the steepest ascent was determined based on comparison of CPE values. The new offset of the center point was recorded. The gradient ascent search is an iterative process and was repeated until no changes of angles and center point offsets were determined. The final iterative values of angles and center point offsets were recorded with their appropriate orientation of the cylinder angle, curvature and cumulative CPE. Then computations were repeated for new set of values for orientation of the cylinder angle and curvature, the values of roll, pitch, yaw were reset to their initial values based on the plane model and center point offsets were nulled. The result of the gradient ascent search was a 3x3 grid model with maximized cumulative measure quantity.

Growing process

The user was asked to pick an initial point on the grid and confirm that the initial 3x3 grid had a proper orientation. Once the first 3x3 grid was approved by user, the growing process was started. The growing process is an independent process and can be parallelized to speed-up grid computations. The growing process consists of two major steps: growing vertically and growing horizontally. These two processes are independent. In this research I suggest averaging the result of the vertical and horizontal growing to improve the final result. The growing process is shown on Figures 10 and 11.

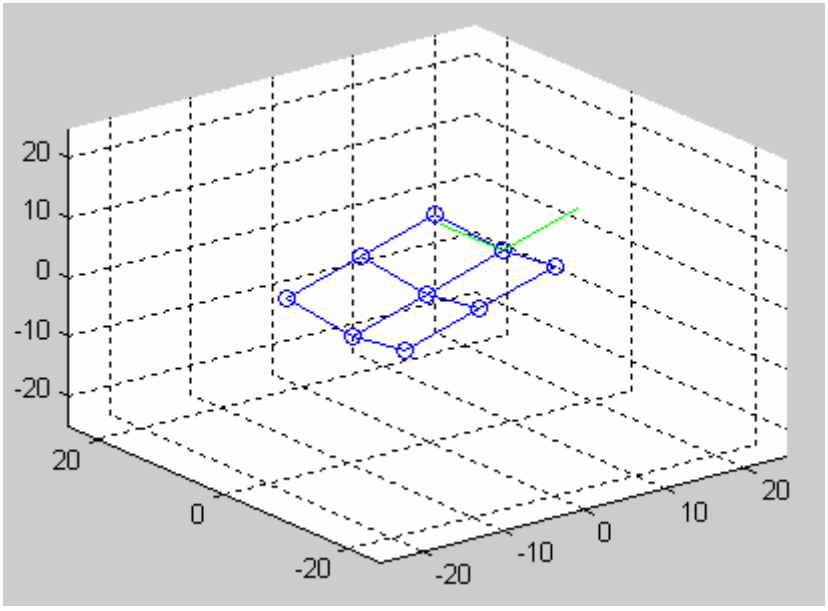

Figure 10. Computation of new local coordinate system ($\vec{u}$ *and* $\vec{v}$ are scaled and shown in green)

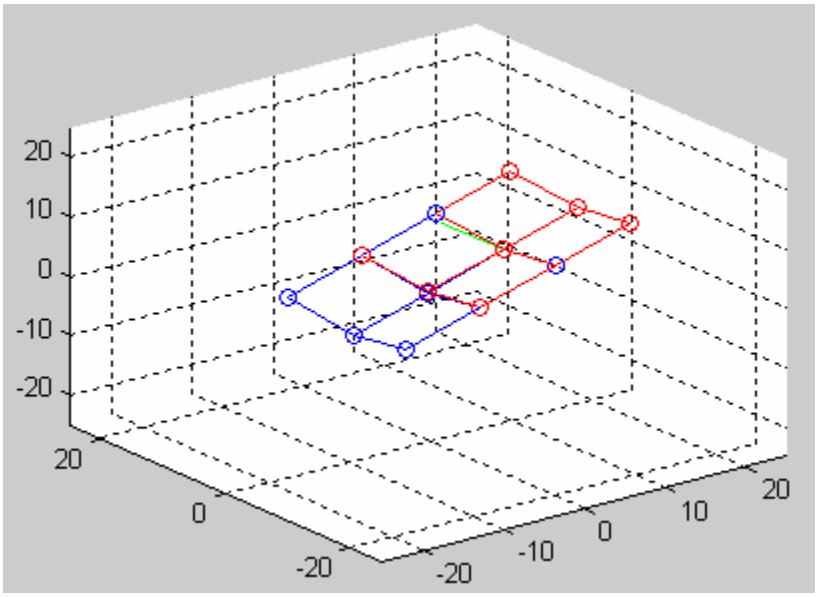

a. Initial orientation of the new 3x3 grid (in red) as extrapolated current 3x3 grid(in blue)

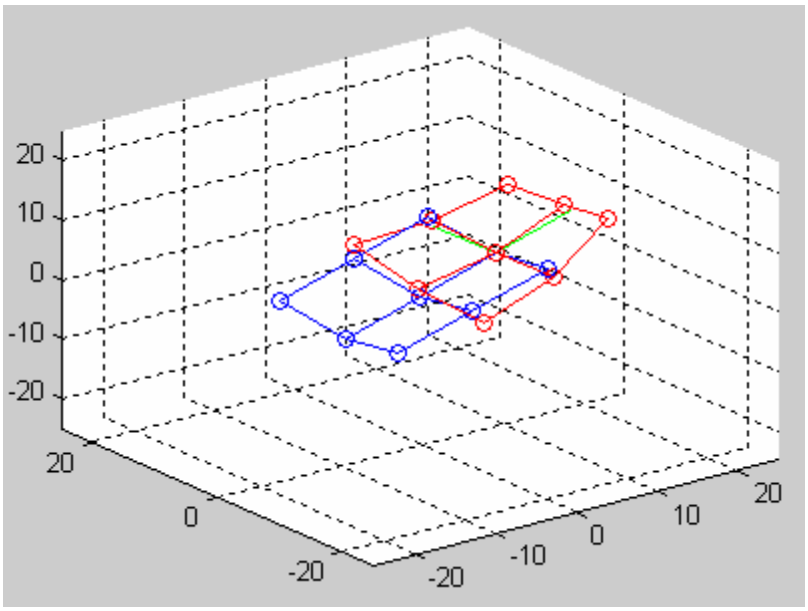

b. Searching for the best fit of the new 3x3 grid (in red), varying all 8 parameters

Figure 11. Growing of the grid

The growing process consists of extrapolation of the grid and performing gradient ascent search on it. The most logical approximation of new 3x3 grid seemed to be

with 4x3 (or 3x4) grid using parameters of current grid. The new 3x3 grid was initialized as the extrapolated part of old 3x3 grid. The initialization was based on the assumption that the curvature and angle of the valley orientation would not change. The roll, pitch and yaw values had to be recomputed since the center of the model was moved. The approximation of the roll, pitch and yaw was done by computing $\vec{u}$ *and* $\vec{v}$ since they are as a local coordinate system in which 3x3 model is specified. To compute the roll, pitch and yaw the rotational matrix R was calculated. The rotational matrix R consisted of three vectors: two orthonormal vectors within plane and the normal vector. To compute two orthonormal vectors at the center of the new grid, the slopes in all three directions were computed [22]. The slope was approximated by:

$$\frac{\partial x}{\partial u} = \frac{x(u_0 + \Delta, v_0) - x(u_0 - \Delta, v_0)}{2 * \Delta}$$

Similarly,

$$\frac{\partial y}{\partial u} = \frac{y(u_0 + \Delta, v_0) - y(u_0 - \Delta, v_0)}{2 * \Delta} \text{ and } \frac{\partial z}{\partial u} = \frac{z(u_0 + \Delta, v_0) - z(u_0 - \Delta, v_0)}{2 * \Delta}$$

The computation of the slope in the direction of the $\vec{v}$ vector was done similarly. Next, $\vec{u}$ *and* $\vec{v}$ vectors were normalized and their cross product yielded the normal vector $\vec{n}$. The rotational matrix R was computed as following

$$\text{R}=\begin{bmatrix} \frac{\partial x}{\partial u} & \frac{\partial x}{\partial v} & n_x \\ \frac{\partial y}{\partial u} & \frac{\partial y}{\partial v} & n_y \\ \frac{\partial z}{\partial u} & \frac{\partial z}{\partial v} & n_z \end{bmatrix}$$

Based on the rotational matrix, the values of roll, pitch and yaw were computed for new 3x3 grid.

Next ascent gradient search similar to the one described above was performed to find the best fit of the 3x3 grid that maximizes the cumulative CPE. To combine current 3x3 grid and new 3x3 grid their overlapping electrode coordinates were averaged.

Growing and Detection of the edges

Since the position of the initial grid relative to the grid is unknown, it was proposed to grow 6 times in vertical and horizontal direction. Step-by-step procedure of growing process is shown on the Figures 12, 13 and 14 below.

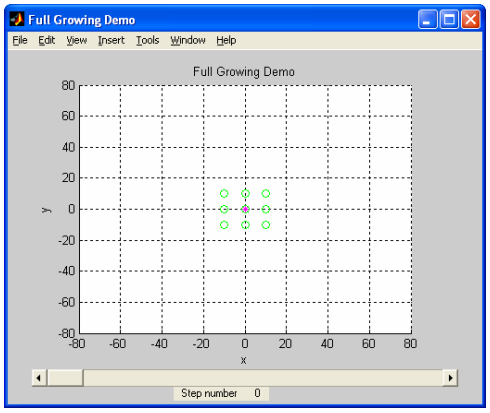

a. Computation of the initial 3x3 grid

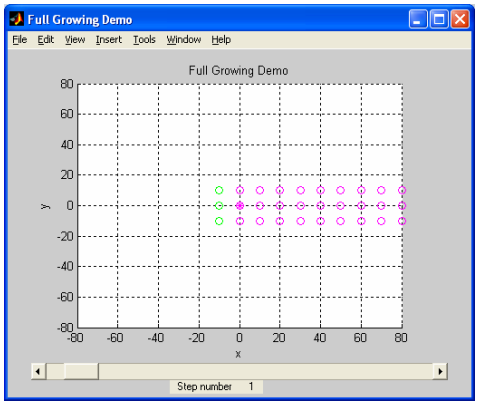

b. Growing in horizontal positive direction

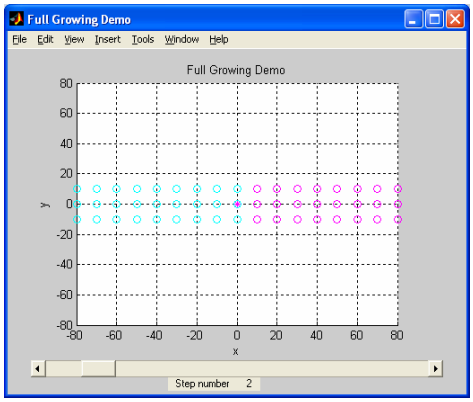

c. Growing in horizontal negative direction

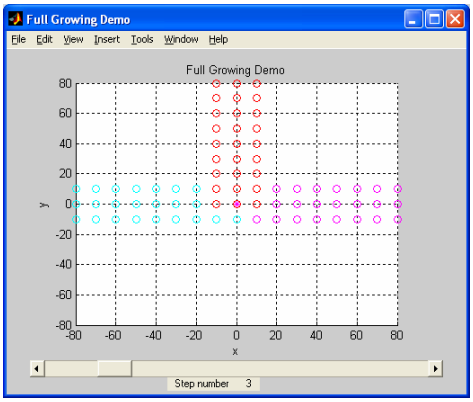

d. Growing in vertical positive direction

Figure 12. Computation of the extensions from center point

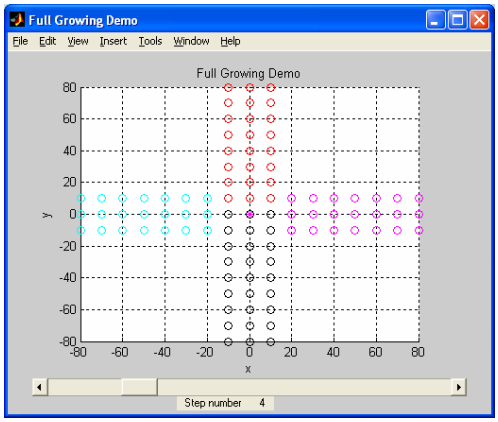

a. All extensions of initial grid in vertical and horizontal directions

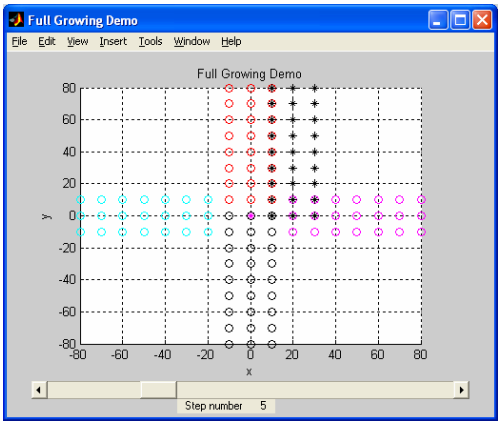

b. Growing in vertical positive using cross as starting point

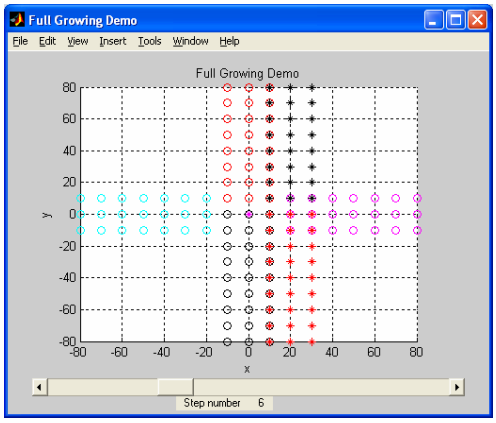

c. Growing in vertical direction using new center point on the cross

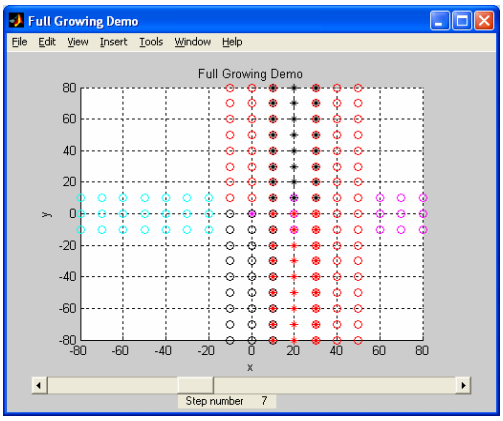

d. Growing in vertical direction further away from origin

Figure 13. Computation of vertical extensions of the cross

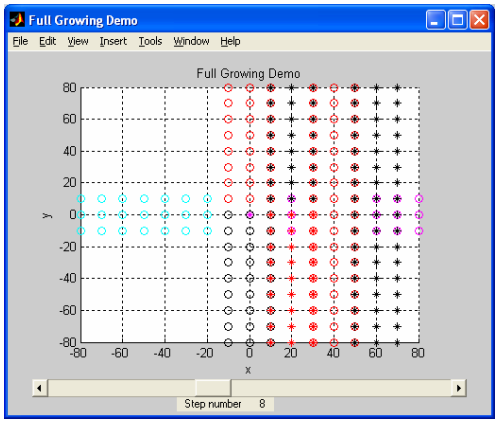

a. More growing in vertical direction

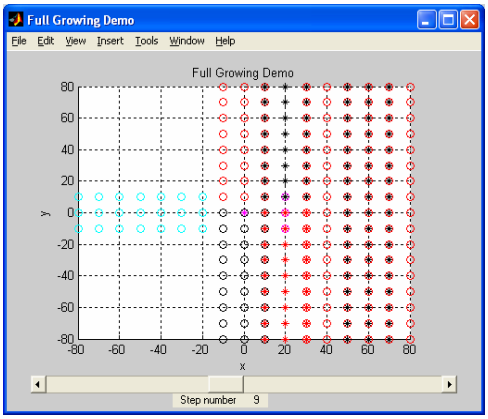

b. Growing in vertical positive direction is complete

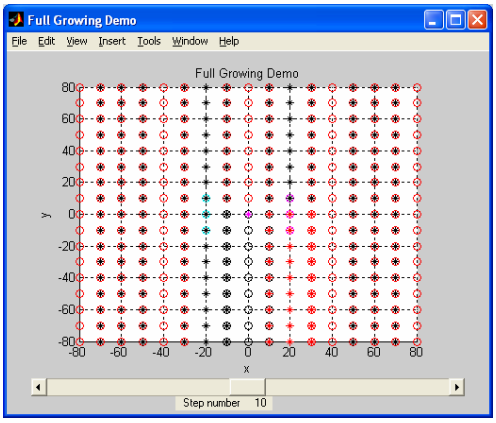

c. Similarly growing was performed in vertical negative direction

Figure 14. Computation of all vertical extensions

Grid was computed as vertical extensions of initial grid. First the vertical and horizontal extensions of the initial grid were computed as shown on Figure 12. The computed extensions create a cross which was used for computation of the full grid. The full grid was computed in two ways and results were averaged. The full 15x15 grid was computed as vertical extension from the initial cross using the cross as a new starting point of growing process as shown on Figure 13. The growing process was performed in such a way that two neighboring grown

extensions would have overlapping edges as shown on Figures 13 and 14. The edges were overlapped to ensure consistent result during growing process. The overlapping points were averaged to insure smoothness of final grid.

Secondly, the cross was used as starting point of extension growing in horizontal direction as shown on Figure 15. Similarly, two neighboring extensions were overlapped and averaged to insure smoothness as shown on Figure 16. Finally, result of vertical and horizontal growing were combined and averaged as shown on Figure 17. The process of averaging between results of vertical and horizontal growing makes each individual extension in either direction to contribute equally to the final result. The final result is less dependent on the errors during computations of the individual 3x3 grids.

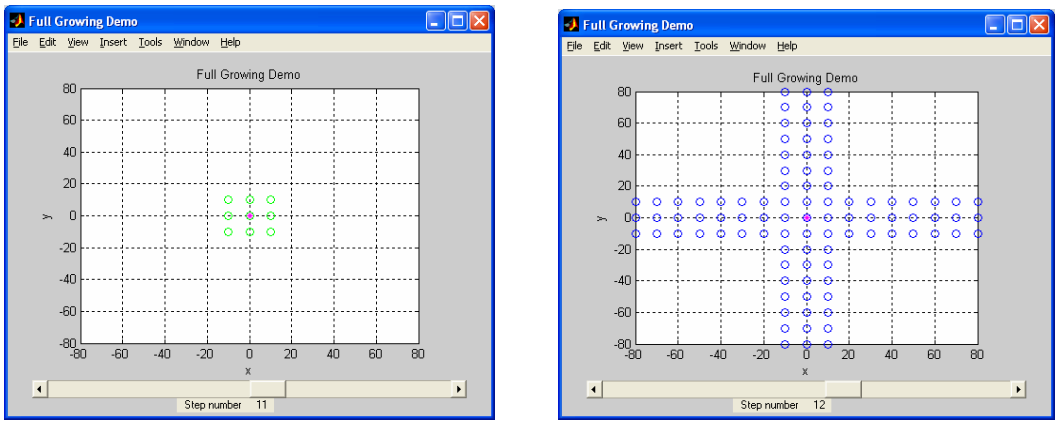

a. Initial grid b. Computed cross

Figure 15. Preliminary computations

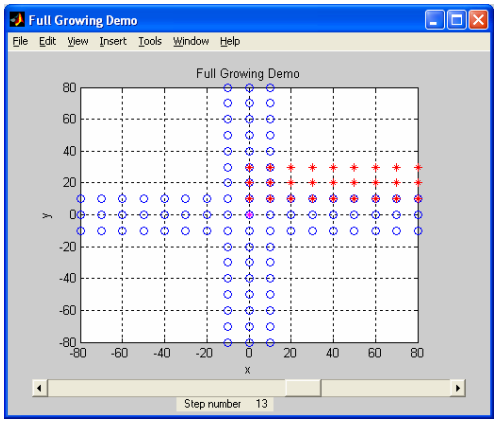

a. Growing from the cross to the right

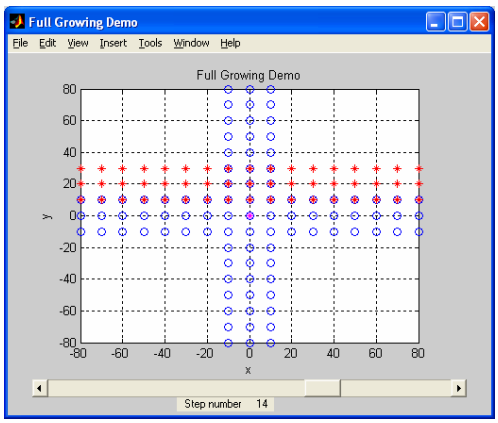

b. Growing from the cross to the left

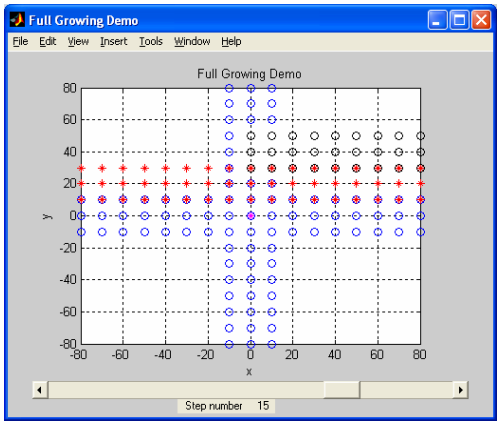

c. Growing in positive horizontal direction further away from center point

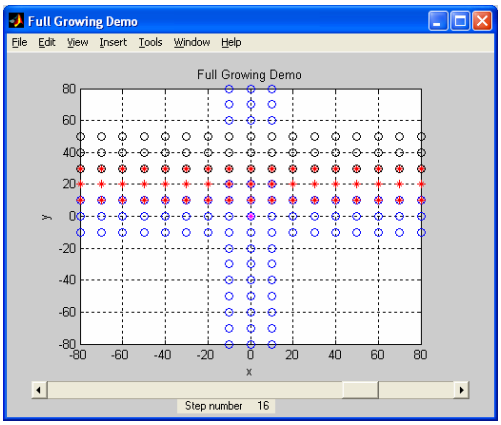

d. Growing in negative horizontal further away from center point

Figure 16. Growing in the horizontal direction

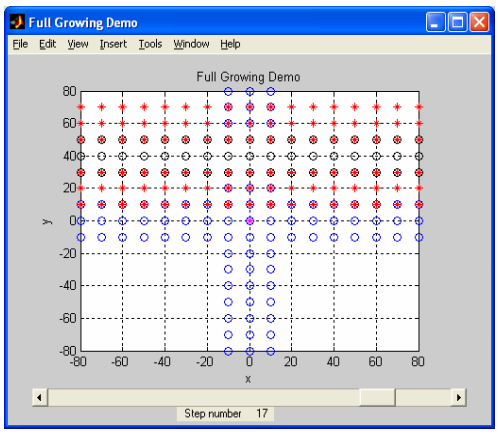

a. More growing in positive horizontal direction

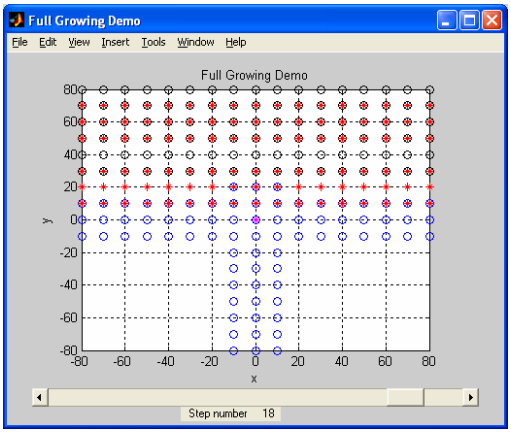

b. Growing in positive horizontal is complete

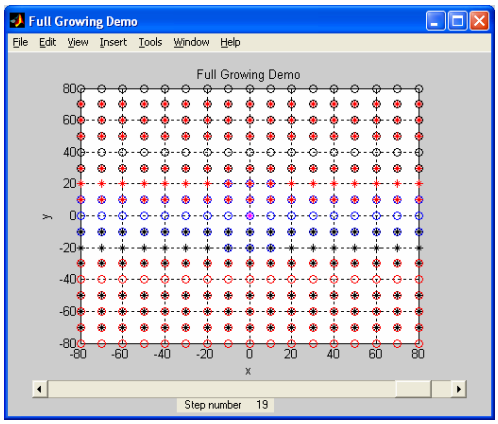

c. Growing in horizontal direction is complete

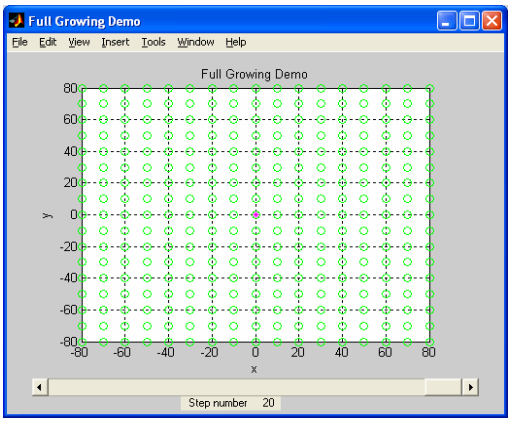

d. Averaging result between horizontal and vertical extensions

Figure 17. Computation of all horizontal extensions and averaging

In this case, no matter where initial grid was located all of the grid would be detected. In addition, the computed grid would extend far beyond the implanted grid and needs to be cropped. To perform cropping of true grid out of grown grid, the search for two rows and two columns with minimum count of dark centers is

performed. For example, if 8x8 grid is being implanted, the search starts to look from left to right for a column with small count of dark spheres followed by the column with relative high dark sphere count. This would indicate x_1 - the left edge of the real grid. In addition, since the length/height of the grid is known, the search also checks for the edge $x_2 = x_1 + L$, where L is length of the implanted grid. If the right edge of the grid is not confirmed by the low number of dark spheres, x_1 is varied. Once both vertical edges were confirmed by the significant decrease in the number of dark spheres in the columns outside of the grid, the extended grid is cropped. Since edges of the grid were initially averaged with the 3x3 grids outside of the implanted, they need to be recomputed. Therefore the two columns of electrode on each side of the cropped grid are computed as horizontal extensions from inside. Similarly, the grid horizontal boundaries were computed, the grid was trimmed to the proper height and edges were recomputed. To insure uniformity and smoothness of the grid the vertical edges were recomputed by averaging with the vertical extension of the 3x3 grid from the center. Similarly for the horizontal edges, they were averaged with horizontal extension of the 3x3 grid from the center.

The final result of LxW grid is displayed in Rex3DViewer where its performance is visually evaluated.

CHAPTER 5

VALIDATION OF THE RESULTS

The validation of the results was done by comparing the results of the algorithm with the electrode centers manual extracted from MRI scan. Due to lack of resources and access to MR scanner, I manually identified and extracted SE from MRI scans. It was a time-consuming, exhaustive and non-trivial process. Some of the artifacts were corrupted by noise to such a high degree that it was unfeasible to recover the electrode center. After the manually extracted electrode centers were compared with the centers generated by the algorithm, numerous mistakes like missing electrodes or electrodes located either too far or too close were discovered in manually extracted data set. The most severe errors were fixed and the distances between manually extracted electrodes and electrode center generated by this algorithm were computed. The statistics of the distances between corresponding points are shown in Table 3.

Table 3. Evaluation of the algorithm against manually extracted points

Statistics of the relative distance in mm	Case 1	Case 3	Case 4
Min	.3584	.4213	.3741
Max	4.5527	4.8953	6.3862
Mean	2.1390	2.4313	2.6432
Median	2.0031	2.2076	2.3128
Standard deviation	1.2518	1.0833	1.4563

In addition, the computed grid was displayed on the screen and visually inspected. The captures for each case are shown on Figures 18, 19 and 20.

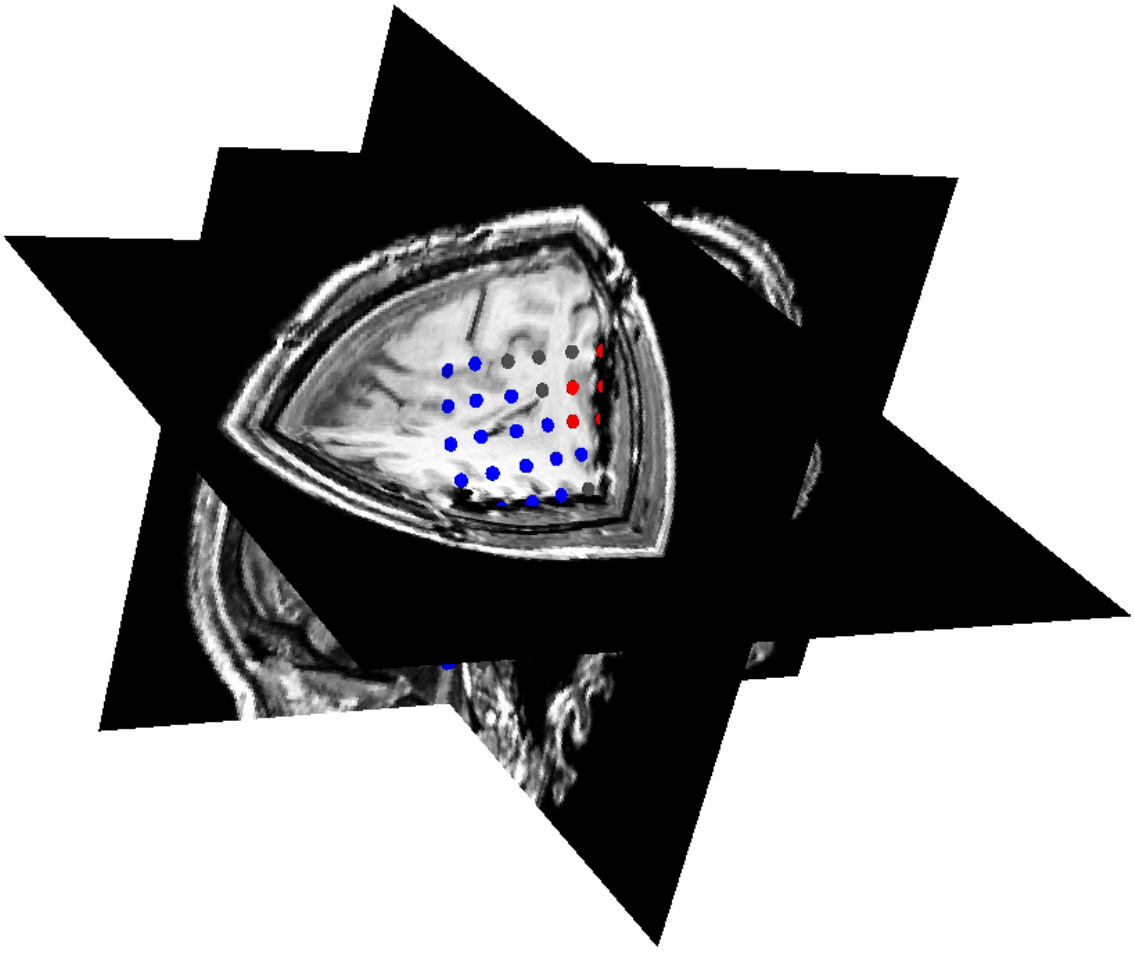

Figure 18. Case 1 with detected 8x10 grid shown (colored electrodes show functional areas)

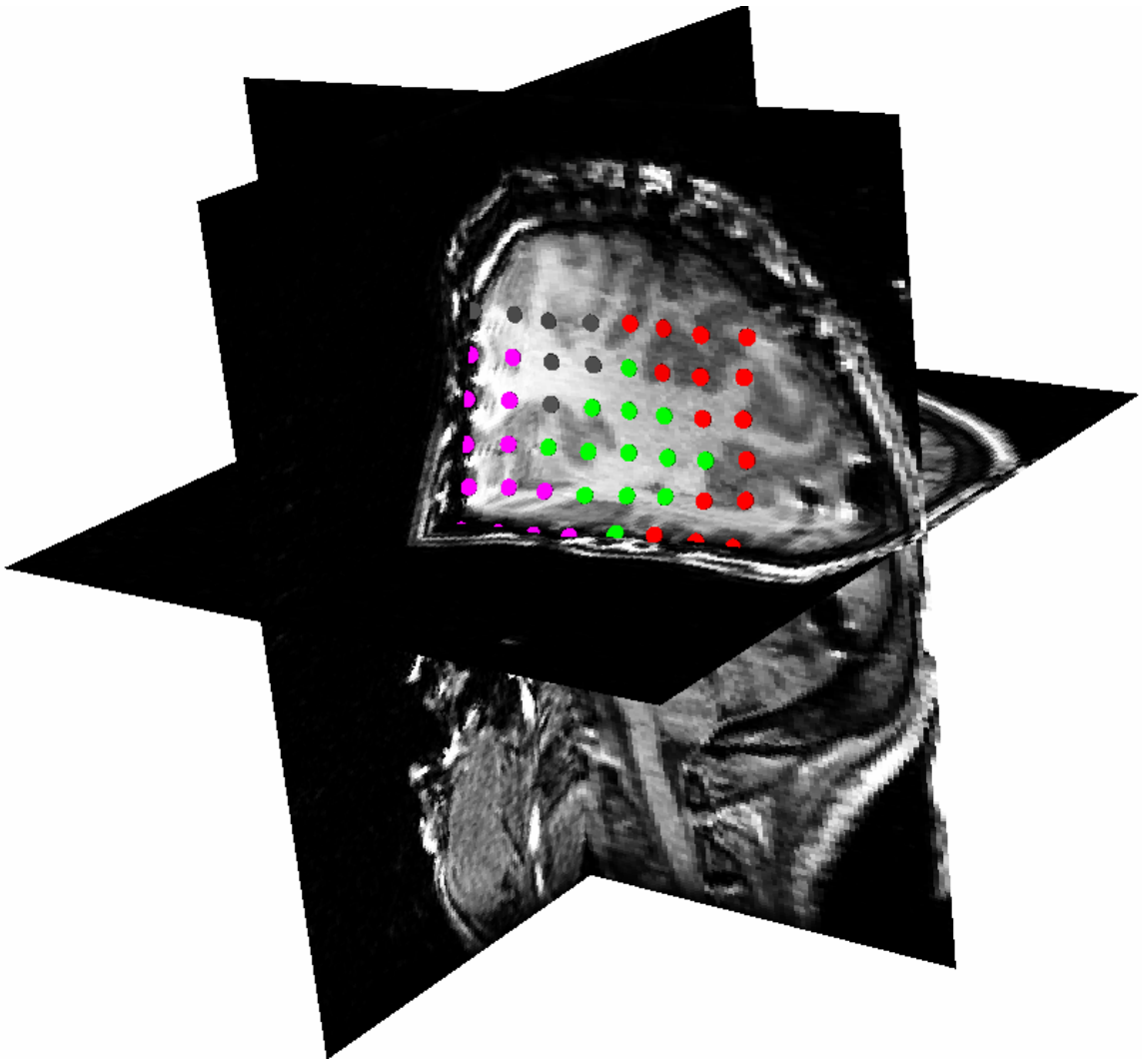

Figure 19. Case 3 with detected 8x8 grid shown (colored electrodes show functional areas)

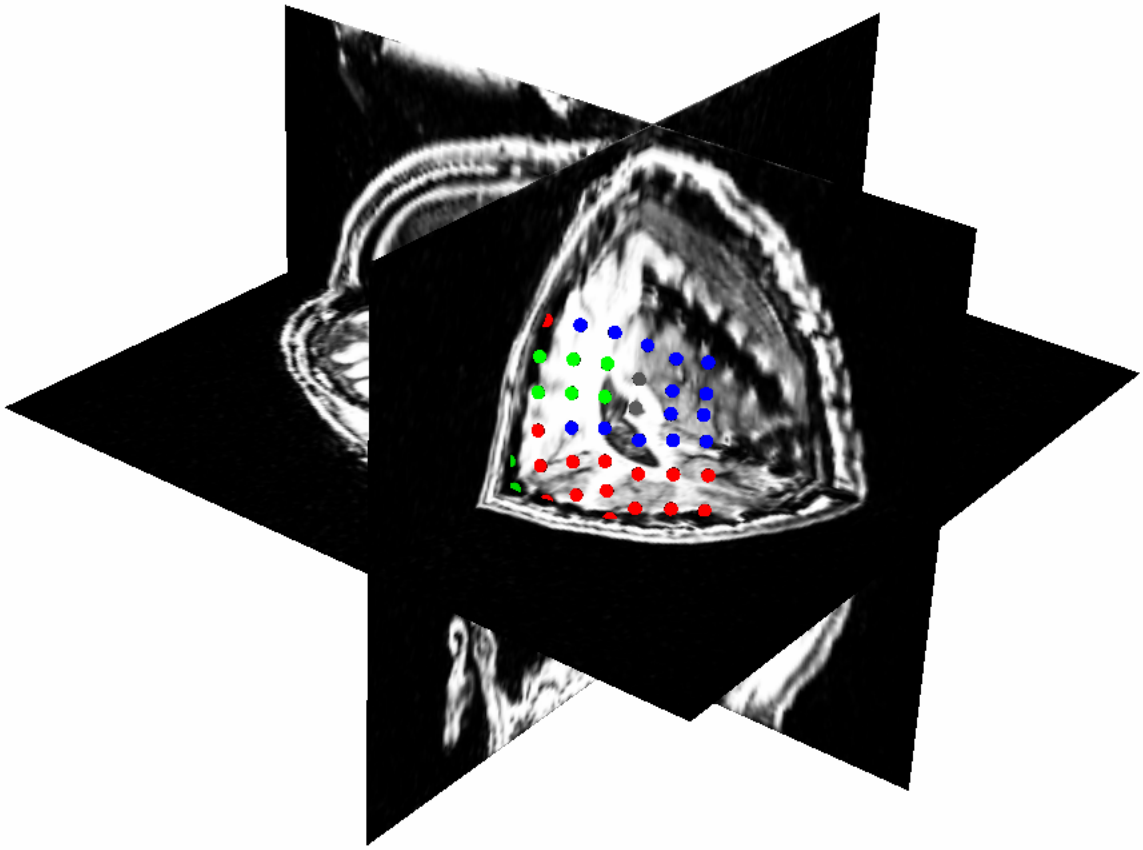

Figure 20. Case 4 with detected 7x9 grid shown (colored electrodes show functional areas)

REFERENCES

[1] Dieter Schmidt, Steven C. Schachter (1999). Epilepsy: problem solving in clinical practice. Martin Dunitz Ltd, 1st edition.

[2] Hans Luders, Youssef G., Md. Comair (2001). Epilepsy Surgery. Lippincott Williams & Wilkins Publishers, 2nd edition.

[3] Atilla Erdem, Ayse Karatas, Gulnihal Kutlu, Ali Savas, Ayse Serdaroglu, Erhan Bilir (2002). Epilepsy and Surgery. Journal of Neurological Sciences. Norol Bil D, Volume 19, Issue 2: April-June 2002, #8. <http://www.med.ege.edu.tr/norolbil/2002/NBD19302.htm>

[4] Oskar Skrinjar and James Duncan, Automatic Extraction of Implanted Electrode Grids, Medical Image Computing and Computer-Assisted Intervention (MICCAI 99), Cambridge, UK, October 1999, pp. 990-997.

[5] Theodore H. Schwartz. Epilepsy-Surgery.com. http://www.epilepsy-surgery.com

[6] Peter W. Kaplan, Pierre Loiseau, Robert S. Fisher, Pierre Jallon (1995). Epilepsy A to Z: A Glossary of Epilepsy Terminology.

[7] David Vossler, Allen R. Wyler (2003). Epilepsy Surgery. eMedicine Health Web Site. <http://www.emedicine.com/med/topic3177.htm>

[8] David Adelson (2004). University of Pittsburgh, Department of Neurological Surgery, Surgical Epilepsy Center. <http://www.neurosurgery.pitt.edu/epilepsy/>

[9] William Bingaman Jr. Epilepsy Surgery Procedures at Cleveland Clinic Comprehensive Epilepsy Center. <http://www.clevelandclinic.org/neuroscience/treat/epilepsy/surgery/>

[10] Oskar Skrinjar and James Duncan, Preserving Intrinsic Surface Distances - Application to Electrode Grid Manipulation, IEEE Workshop on Mathematical Methods in Biomedical Image Analysis (MMBIA 2000), Hilton Head Island, SC, USA, June 2000, pp. 54-60

[11] Peggy Woodward (2000). MRI for Technologists. McGraw-Hill/Appleton & Lange; 2nd edition.

[12] Andrew G. Webb. (2002). Introduction to Biomedical Imaging. John Wiley & Sons.

[13] Isaac Bankman. (2000). Handbook of Medical Imaging: Processing and Analysis. Academic Press, 1st edition.

[14] B. Dogdasa, D. Shattuckb, and R. M. Leahyc. Segmentation of Skull in 3D Human MR Images Using Mathematical Morphology. Signal and Image Processing Institute, University of Southern California.

[15] Mark J. Smith, Alen Docef. (1997). A Study Guide for Digital Image Processing. Scientific Publishers, Incorporated, 1st edition.

[16] V.F. Leavers (1992). Shape Detection in Computer Vision Using the Hough Transform. Springer-Verlag Berlin and Heidelberg GmbH & Co.

[17] William H. Press, Brian P. Flannery, Saul A. Teukolsky, William T. Vetterling (1992). Numerical Recipes in C: The Art of Scientific Computing. Cambridge University Press, 2nd edition.

[18] Eric Weisstein (2004). The Web's Most Extensive Mathematics Resource. <http://mathworld.wolfram.com/>

[19] T. Kirkman (2004). Tools for Science. <http://www.physics.csbsju.edu>

[20] Michael Gerke (2001). Modeling and Simulation of Robotic Systems. <http://prt.fernuni-hagen.de/lehre/KURSE/PRT001>

[21] Diana Gruber (2000). The Mathematics of the 3D Rotation Matrix. <http://www.makegames.com/3drotation/>

[22] Richard Gourdeau (2004). A Robotics Object Oriented Package in C++. <http://www.cours.polymtl.ca/roboop/docs/robot.html>

[23] William R. Hendee, E. Russell Ritenour (2002). Medical Imaging Physics. Wiley-Liss, 4th edition.

[24] Jerrold T. Bushberg, J. Anthony Seibert, Edwin M. Leidholdt Jr., John M. Boone. (2001). The Essential Physics of Medical Imaging. Lippincott Williams & Wilkins Publishers, 2nd Edition.

[25] P. Janin. (2003). Terminology and Methodology for Validation in Medical Image Processing. (MICCAI 2003), Laboratoire IDM Faculté de Médecine Université de Rennes, France.